Structure of Coenzyme A−Disulfide Reductase from *Staphylococcus aureus* at 1.54 Å Resolution[†,‡]

T. Conn Mallett,[§,||,⊥] Jamie R. Wallen,[§,||] P. Andrew Karplus,[#] Hiroaki Sakai,[△,⊗] Tomitake Tsukihara,[△] and Al Claiborne*[,§]

Center for Structural Biology, Wake Forest University School of Medicine, Winston-Salem, North Carolina 27157, Department of Biochemistry and Biophysics, Oregon State University, Corvallis, Oregon 97331, and Institute for Protein Research, Osaka University, Suita, Osaka 565-0871, Japan

Received June 8, 2006; Revised Manuscript Received July 27, 2006

ABSTRACT: Coenzyme A (CoASH) replaces glutathione as the major low molecular weight thiol in *Staphylococcus aureus*; it is maintained in the reduced state by coenzyme A−disulfide reductase (CoADR), a homodimeric enzyme similar to NADH peroxidase but containing a novel Cys43-SSCoA redox center. The crystal structure of *S. aureus* CoADR has been solved using multiwavelength anomalous dispersion data and refined at a resolution of 1.54 Å. The resulting electron density maps define the Cys43-SSCoA disulfide conformation, with Cys43-S_γ located at the flavin *si* face, 3.2 Å from FAD-C4aF, and the CoAS-moiety lying in an extended conformation within a cleft at the dimer interface. A well-ordered chloride ion is positioned adjacent to the Cys43-SSCoA disulfide and receives a hydrogen bond from Tyr361′-OH of the complementary subunit, suggesting a role for Tyr361′ as an acid−base catalyst during the reduction of CoAS−disulfide. Tyr419′-OH is located 3.2 Å from Tyr361′-OH as well and, based on its conservation in known functional CoADRs, also appears to be important for activity. Identification of residues involved in recognition of the CoAS−disulfide substrate and in formation and stabilization of the Cys43-SSCoA redox center has allowed development of a CoAS-binding motif. Bioinformatics analyses indicate that CoADR enzymes are broadly distributed in both bacterial and archaeal kingdoms, suggesting an even broader significance for the CoASH/CoAS−disulfide redox system in prokaryotic thiol/disulfide homeostasis.

In contrast to the central role played by the tripeptide thiol glutathione [GSH (*1*)] in maintaining thiol/disulfide homeostasis and providing an important line of antioxidant defense in, for example, *Escherichia coli*, earlier studies clearly indicated the absence of GSH in a number of bacteria (*2*, *3*) and in all archaea (*4*, *5*). Coenzyme A (CoASH) was shown to be the major low molecular weight thiol in *Bacillus megaterium* (*3*) and *Deinococcus radiodurans* (*2*), as well as in the human pathogen *Staphylococcus aureus* (*6*). Reinforcing the concept that CoASH assumes the intracellular redox function of GSH in *S. aureus*, a novel NADPH-dependent flavoprotein disulfide reductase, coenzyme A−disulfide reductase (CoADR),[1] was identified (*6*, *7*). Consistent with the important functional role attributed to CoADR, staphylococcal virulence in mice was shown to be attenuated for CoADR-deficient strains (*8*, *9*).

In 2001, Dym and Eisenberg (*10*) defined two subfamilies within the glutathione reductase (GR) family, based on sequence−structure analyses of FAD-binding folds; the GR_1 subfamily includes all of the functional pyridine nucleotide disulfide oxidoreductases [PNDORs (*11*)]. Argyrou and Blanchard (*12*) subsequently noted that the PNDORs could

[†] This work was supported by National Institutes of Health Grant GM-35394 (A.C.), by National Science Foundation Grant INT-9803674 (A.C.), by grants-in-aid from the Ministry of Education, Culture, Sports, Science, and Technology (Monbusho), Japan, and the Japan Society for the Promotion of Science (T.T.), and by National Science Foundation Grant MCB-9982727 (P.A.K.). T.C.M. was the recipient of International Fellowship P-99934 from the Japan Society for the Promotion of Science. A.C. was the recipient of Short-Term Invitation Fellowship RC20137002 from the Japan Society for the Promotion of Science. Data for this study were measured at beamline X26C of the National Synchrotron Light Source. Financial support comes principally from the Offices of Biological and Environmental Research and of Basic Energy Sciences of the U.S. Department of Energy and from the National Center for Research Resources of the National Institutes of Health.

[‡] Coordinates have been deposited with the Protein Data Bank under the file name 1YQZ.

* To whom correspondence should be addressed. Tel: (336) 716-3914. Fax: (336) 777-3242. E-mail: alc@csb.wfu.edu.

[§] Wake Forest University School of Medicine.

[||] These authors contributed equally to this work.

[⊥] Present address: Rigaku, Sevenoaks, Kent TN15 6QY, England.

[#] Oregon State University.

[△] Osaka University.

[⊗] Present address: RIKEN Genomic Sciences Center, Yokohama City, Kanagawa 230-0045, Japan.

[1] Abbreviations: CoADR, coenzyme A−disulfide reductase; GR, glutathione reductase; PNDOR, pyridine nucleotide disulfide oxidoreductase; Npx, NADH peroxidase; Nox, NADH oxidase; CoAD, coenzyme A−disulfide; EH_2, two-electron-reduced enzyme; HEPES, *N*-(2-hydroxyethyl)piperazine-*N*′-2-ethanesulfonic acid; PEG, polyethylene glycol; SeMet, selenomethionine; NCS, noncrystallographic symmetry; MAD, multiwavelength anomalous dispersion; TrxR, thioredoxin reductase; Cys44-SO_2H, Cys44-sulfinic acid; DBM, dinucleotide-binding motif; CoAS-I and CoAS-II, the assigned halves of modeled coenzyme A−disulfide; Cys-SOH, cysteine-sulfenic acid; BACoADR, *Bacillus anthracis* coenzyme A−disulfide reductase; SACoADR, *Staphylococcus aureus* coenzyme A−disulfide reductase; RHD, rhodanese homology domain.

10.1021/bi061139a CCC: $33.50
Published on Web 08/31/2006

be subdivided on the basis of mechanistic and sequence−structural information into three groups, with "group 3" including CoADR, NADH peroxidase (Npx), and NADH oxidase (Nox). Until the identification of CoADR (*6*), all flavoprotein disulfide reductases were members of PNDOR groups 1 and 2, and all group 3 enzymes were specific for either H_2O_2 or O_2 ($\rightarrow 2H_2O$) reduction. CoADR is clearly by sequence a group 3 PNDOR enzyme (*7*); it (like Npx and Nox) differs fundamentally from the other PNDOR groups in the *absence* of the primary cystine−disulfide redox center (*13*). In contrast with Npx and Nox, however, the single active site Cys43 of CoADR is able to reduce the CoAS−disulfide (CoAD) substrate via formation of a Cys43-SSCoA mixed disulfide that also represents the stable oxidized form of the enzyme as purified from either *S. aureus* or recombinant *E. coli* (*14*). GR is one of the best characterized members of PNDOR group 1; like CoADR, GR reduces its low molecular weight disulfide substrate (GSSG) with reducing equivalents derived from NADPH. Unlike CoADR, GR contains a redox-active protein disulfide, in addition to FAD. NADPH binds at the flavin *re* face, and electrons flow through the FAD isoalloxazine, leading to reduction of the redox-active disulfide (Cys58-SS-Cys63, in human erythrocyte GR). Each nascent Cys-SH has a distinct catalytic role: Cys58, the interchange thiol, serves as the nucleophile which attacks the GSSG substrate, forming the Cys58-SSG mixed disulfide intermediate. Cys63, the charge-transfer thiol, is characterized by a low pK_a; the Cys63−thiolate is responsible for the electronic interaction with the oxidized flavin that imparts the long-wavelength absorbance band centered at ~530 nm in the two-electron reduced (EH_2; FAD, 2 Cys-SH) enzyme. This Cys63−thiolate also reacts with the Cys58-SSG intermediate to restore the redox-active disulfide in the fully oxidized enzyme. Two GSH are released per catalytic cycle, and His467′ (His439′ in *E. coli* GR) plays an essential role in protonating the GS-I thiolate as the Cys58-Cys63 disulfide is formed.

Mechanistically, since the functional equivalent of the charge-transfer cysteine is absent in CoADR, the Cys43-SSCoA mixed disulfide must be reduced by NADPH (via the flavin). In terms of its redox and spectroscopic properties, as assessed in reductive titrations, CoADR offers two additional contrasts with GR: (1) although the CoADR EH_2 intermediate is formally equivalent to that of GR, dithionite titrations do not yield the characteristic charge-transfer species, and (2) NADPH titrations of CoADR reveal strong active site asymmetry; only one FAD of the homodimer is reduced at equilibrium, with the physiological substrate.

We have undertaken structural studies of *S. aureus* CoADR in order to elucidate the origins of these catalytic and redox properties that distinguish this enzyme from all other members of the PNDOR family, combining the low molecular weight disulfide substrate preferences of group 1 enzymes with structural features of the group 3 Npx and Nox enzymes. Here, we report the crystal structure of native, oxidized *S. aureus* CoADR, refined at 1.54 Å resolution. Of particular interest is the active site Cys43-SSCoA redox center, which identifies the residues involved in CoAS-recognition and guides insights into the mechanism of CoAD reduction. The structural and functional divergence between CoADR and Npx/Nox, within the PNDOR group 3, has also allowed the identification of CoADR homologues among several biodefense pathogens and numerous archaea.

EXPERIMENTAL PROCEDURES

Protein Purification and Crystallization. Expression and purification of *S. aureus* CoADR followed published protocols (*14*). Purified enzyme, in 10 mM sodium HEPES, pH 7.0, was screened for crystallization at 20 °C using hanging drops (2 μL of protein sample plus 2 μL of reservoir solution, final protein concentration of 10 mg/mL) and the sparse-matrix strategy (*15*) implemented in Crystal Screens I and II (Hampton Research, Inc.). Large, single crystals of CoADR grew best in the presence of 1.3 mM $NADP^+$, using a reservoir solution of 33−43% PEG 400, 0.2−0.4 M $MgCl_2$, and 0.1 M HEPES (pH 7.0−7.5). Crystals appeared within 1 day, growing to full size (~0.3 mm × 0.4 mm × 0.5 mm) in 1 week, and were flash-frozen in a nitrogen stream at 100 K after being removed from the drop. SeMet-substituted CoADR was expressed in the methionine auxotroph B834-(DE3), essentially as described by Wood et al. (*16*) for *Salmonella typhimurium* AhpF. SeMet CoADR was purified and crystallized in the same manner as the native protein.

Data Collection, Structure Solution, and Refinement. The crystals belong to space group $P2_1$, with $a = 76.1$ Å, $b = 65.2$ Å, $c = 94.5$ Å, and $\beta = 104.8°$; there are two 51 kDa monomers in the asymmetric unit. Multiwavelength diffraction data with the SeMet crystals (Table 1) were processed using the programs MOSFLM (*17*) and SCALA (*18*, *19*) in the CCP4 suite (*20*). SOLVE (*21*) was used to locate 16 of the 18 Se sites, and these coordinates were used for phase calculation in SHARP [Table 1 (*22*)]. The local NCS matrix of the heavy atom sites was determined using the programs POLARRFN and GETAX in the CCP4 suite. The initial phases were improved using DM (*23*), through solvent flattening, histogram matching, and NCS averaging. The resulting electron density map allowed 70% of each monomer to be built automatically using MAID (*24*). The remaining residues were manually built using *O* (*25*). A number of native data sets were collected and analyzed during the early stages of refinement; we report statistics only for the data sets used in the final refinement (native1) and for calculation of an anomalous map to confirm chloride positions (native2). All native data were processed with d*TREK (*26*). Refinement was carried out using CNS (*27*) with cycles of simulated annealing, with both positional and temperature factor refinements followed by manual rebuilding into composite omit maps calculated by CNS. The topology and parameter files for FAD and CoASH required for CNS were constructed using XPLO2D (*28*). Water molecules were identified by CNS, using a 3σ difference Fourier cutoff, and were visually confirmed. In the later stages of refinement, three magnesium ions were added to the model on the basis of strong electron density peaks, as coordinated with octahedral geometry to solvent water molecules, and six chloride ions were identified on the basis of the strength of $F_o - F_c$ electron density, significant ($>6\sigma$) peaks in an anomalous map, hydrogen-bonding distances, and *B*-factors similar to those of surrounding atoms. A total of 1363 solvent water molecules were added to the model, with favorable hydrogen-bonding interactions and peaks greater than 0.5σ in the $2F_o - F_c$ electron density map.

Table 1: Data Collection and Phasing Statistics

	native1[a]	native2[b]	edge[c]	peak[c]	remote[c]
wavelength (Å)	1.1000	1.5418	0.9799	0.9762	0.9000
resolution (Å)	1.54	1.89	2.50	2.70	2.50
reflections	942329	892209[d]	170804	135526	153427
unique reflections	131158	140099[d]	29437	23369	29357
completeness (%)	99.6 (96.6)[e]	100.0 (99.7)[d]	99.9 (99.9)	99.9 (99.9)	99.9 (99.9)
R_{meas} (%)[f]	7.8 (35.6)[g]	7.9 (41.9)[g]	9.2 (34.1)	10.3 (26.0)	9.4 (26.6)
phasing power			4.04	3.72	
resolution range (Å)			20.0−2.7	20.0−2.7	20.0−2.7
R_{Cullis}[e]			0.35	0.36	
R_{Cullis} (anomalous)			0.95	0.77	0.92
figure of merit			0.50		

[a] Collected at beamline X26C of the National Synchrotron Light Source (Brookhaven National Laboratory) using an ADSC Quantum-4 CCD detector. [b] Collected on a Rigaku Saturn-92 CCD detector using Cu Kα radiation from a MicroMax-007 rotating anode X-ray generator. [c] Collected using the 3 × 3 CCD detector PX210 (Oxford) at undulator beamline BL44XU of SPring-8, Hyogo, Japan. [d] Completeness and redundancy statistics reflect treatment of I^+ and I^- as nonequivalent reflections in order to evaluate anomalous differences. [e] Numbers in parentheses represent data for the highest resolution shell. [f] R_{meas} is the multiplicity-weighted merging *R*-factor of Diederichs and Karplus (*19*). [g] Data were scaled and merged using d*TREK; unmerged profile-fitted reflections were imported into MTZ format for a run of SCALA to calculate R_{meas}.

Structure superpositions were performed using the DALI server (*29*) and LSQKAB (*30*).

RESULTS AND DISCUSSION

Structure Solution and Quality of the Model. Molecular replacement searches using AMoRe (*31*) and CNS with either Npx (PDB code 1JOA) or Nox (PDB code 2BC0) as search models gave no solution resulting in an interpretable electron density map. Thus, a three-wavelength MAD data set was collected using SeMet CoADR crystals in order to solve the structure. A total of 16 Se sites were identified, and the experimental MAD-phased electron density map calculated at 2.7 Å resolution showed continuous electron density for the protein backbone and allowed identification of most side chain positions. The crystal structure of CoADR reveals one symmetrical dimer (chains A and B) in the asymmetric unit, consistent with the quaternary structures observed with nearly all PNDOR enzymes (*11*). Both polypeptide chains are clearly defined in the electron density and have similar average *B*-factors of 17 and 18 Å^2, respectively. Less well-defined regions of the protein involve two different segments with solvent-exposed loops, residues 51−61 in chain A with an average *B*-factor of 34 Å^2 and residues 361−378 in chain B with an average *B*-factor of 24 Å^2. These two regions are better ordered in the corresponding complementary subunits with average *B*-factors of 21 and 14 Å^2, respectively, owing in large part to crystal contacts with symmetry mates. These variations are therefore attributed to different crystal-packing environments rather than to intrinsic structural differences between the A and B chains. Although NCS restraints were not used during refinement with the 1.54 Å data, the two subunits are virtually identical with an overall C_α rmsd of 0.47 Å; detailed descriptions of the structure will primarily focus on the active site of chain A, with residues from chain B being designated by a prime symbol (e.g., Cys43 = chain A; Cys43′ = chain B). The final model, comprising residues 2−438 for both subunits, 2 FAD cofactors, 2 covalently bound CoAS-, 1363 solvent waters, 6 chloride ions, and 3 magnesium ions, yielded an *R*-factor of 17.7% (R_{free} = 20.6%) with good geometry (Table 2). The refined structure clearly establishes the identity of the residue at position 168 as Tyr, not Asn as reported from the original DNA sequence (*7*). We were able to confirm the validity of Tyr168 by resequencing the CoADR expression plasmid, which had been obtained from delCardayré et al. (*7*). A Luzzati plot (*32*) gives an estimated coordinate error of 0.14 Å for the well-ordered parts of the model. The $2F_o - F_c$ map in the active site region also illustrates the accuracy of the final refined model (Figure 1).

Table 2: Crystallographic Refinement Statistics

resolution range (Å)	10−1.54
amplitude cutoff	none
no. of amino acid residues	874
no. of magnesium ions	3
no. of chloride ions	6
no. of waters	1363
no. of total non-hydrogen atoms	8506
average *B*-factor (Å^2)	20.8
protein	17.9
FAD-binding domain	17.3
NADPH-binding domain	19.4
Interface domain	17.1
solvent	35.0
R-factor (%)	17.7
R_{free} (%)	20.6
stereochemical ideality	
bond length rmsd (Å)	0.010
bond angle rmsd (deg)	1.60
φ,ψ most favored (%)	88.4
φ,ψ additionally allowed (%)	10.7
φ,ψ generously allowed (%)	0.9

Overall Structure. The overall structure of CoADR (Figure 2) is very similar to that of Npx (*33*) and, by extension, to that of GR (*34*, *35*), the best characterized PNDOR enzyme. The CoADR monomer consists of three domains, the two-part FAD-binding domain (residues 1−114 and 242−319), the NADPH-binding domain (residues 115−241), and the C-terminal Interface domain (residues 323−438). In the earlier GR and Npx structure reports, the C-terminal segment of the FAD-binding domain was designated as a distinct "Central" domain. The incorporation of this segment into the currently defined FAD-binding domain originated with the *E. coli* GR structure (*36*), and here we additionally define the N-terminal and C-terminal segments as "FAD-1" and "FAD-2." The three-domain architecture is strongly conserved and has been described in detail for several PNDORs, including *E. coli* GR [group 1 (*36*)] and mammalian TrxR [group 2 (*37*)], as well as for other members of the GR_1 subfamily (*10*). As recently analyzed, this subfamily includes

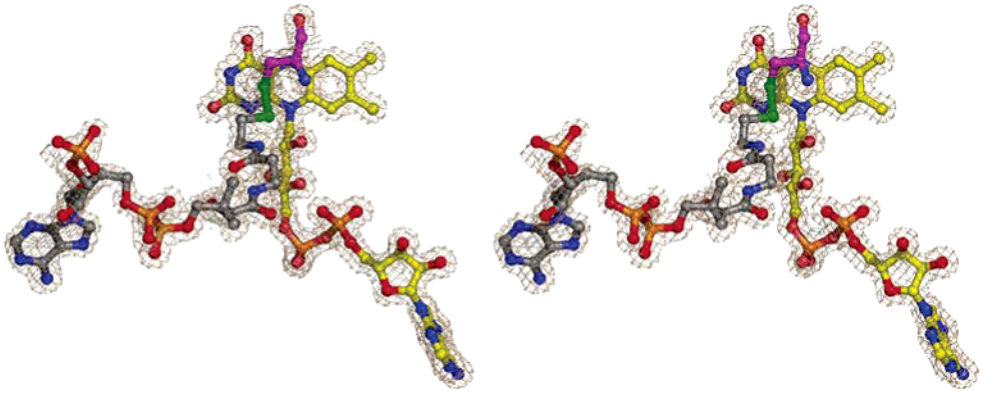

FIGURE 1: Final $2F_o - F_c$ map, in stereo, for the full FAD and Cys43-SSCoA redox centers of chain A, together with the refined model. All carbon atoms are color-coded as follows: CoAS-, gray; Cys43, magenta; FAD, yellow. All other residues are color-coded by atom type. The depicted contour level is 1σ.

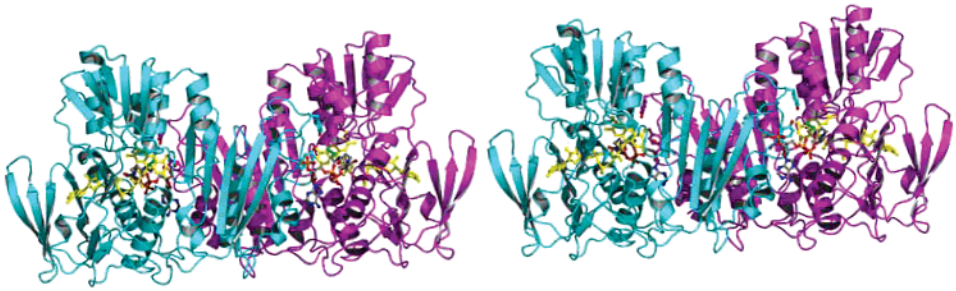

FIGURE 2: Stereoview of the CoADR dimer, colored by subunit: chain A, magenta; chain B, cyan. CoAS- color coding is as in Figure 1, FAD is in yellow, and Cys43, Tyr361, and Tyr419 side chain carbon atoms are colored by subunit.

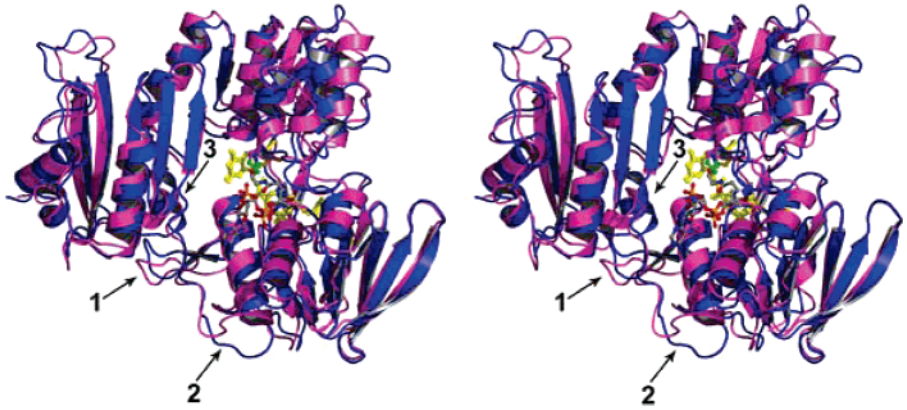

FIGURE 3: Superposition, in stereo, of CoADR chain A (magenta) with an Npx (1JOA) monomer (blue). The DALI server gives rmsd = 2.1 Å for 433 C_α atoms with 25% sequence identity. Cys43-SSCoA and FAD are color-coded as in Figure 2; Npx Cys42-SOH C_β is in blue, with other elements color-coded by atom type. Main chain differences between CoADR and Npx are indicated by arrows for CoADR segments 284−288 (1), 309−315 (2), and 337−349 (3).

functionally diverse proteins such as glutamate synthase, adrenodoxin reductase, and cyclohexanone monooxygenase. The FAD- and NADPH-binding domains of CoADR both have canonical Rossmann folds (*38*); each consists of a central five-stranded parallel β-sheet, with a three-stranded antiparallel β-sheet packed on one side of the central sheet and several α-helices on the opposite side. CoAS- is associated with a cleft at the dimer interface; this cleft is formed by portions of the FAD-binding domain of chain A and the Interface domain of chain B, which contains a large five-stranded antiparallel β-sheet with three short α-helices at the C-terminus. The dimer interface, with a total buried surface area of 2652 Å^2 per monomer, is L-shaped; direct contacts between the respective Interface domains contribute 50% of the total buried surface area, with contacts between each Interface domain and elements of the respective FAD-binding domain providing the remainder. The Interface domain is involved in all of the significant intersubunit contacts.

When the DALI server is used to search the RCSB structure database, Npx is identified as the protein whose structure is most similar to that of CoADR (Figure 3), with C_α rmsd = 2.1 Å for 433 atoms. A similar superposition with the wild-type (Cys44-SO_2H) *Streptococcus pyogenes* Nox structure (PDB code 2BC0) gives a C_α rmsd = 2.1 Å for 431 atoms. The only significant main chain differences between CoADR and Npx appear in two surface-exposed segments corresponding to residues 284−288 and 309−315 in CoADR. In the NADPH-binding domain, CoADR has a four-residue deletion (corresponding to Npx residues 119−122) at its start; this corresponds to a slight shift in the α-helix of the $\beta\alpha\beta$ fold, away from the FAD-1 segment,

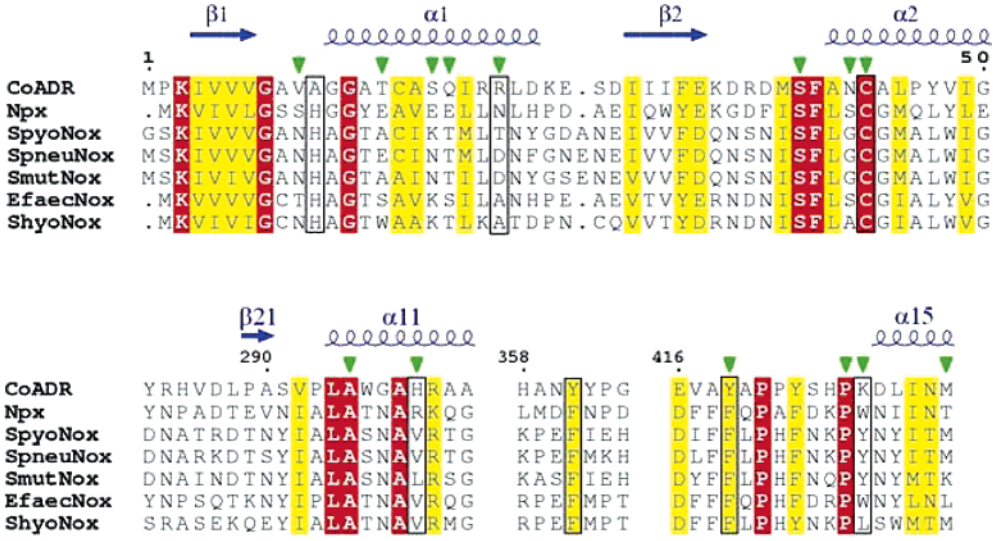

FIGURE 4: Structure-based sequence alignment for CoADR, Npx, and five known functional Nox ($O_2 \rightarrow 2H_2O$) proteins. Npx is from *Enterococcus faecalis* 10C1 [Efaec (*41*)]; Nox sequences correspond to *S. pyogenes* [Spyo (*42*)], *Streptococcus pneumoniae* [Spneu (*43*)], *Streptococcus mutans* [Smut (*44*)], *E. faecalis* (*45*), and *Brachyspira* (formerly *Serpulina*) *hyodysenteriae* [Shyo (*46*)]. Structures have been determined for CoADR (this work), for Npx (1NPX and 1JOA), and for SpyoNox (2BC0). Residue numbering and secondary structure assignments correspond to CoADR; inverted triangles correspond to protein−CoAS- contacts for CoADR (see Figure 5). Red and yellow blocks correspond to absolutely conserved residues and conservative substitutions, respectively. CoADR Ala11, Arg22, Cys43, His299, Tyr361, Tyr419, and Lys427 are highlighted in boxes. Aligned sequence segments correspond to the FAD-1 subdomain, part of the FAD-2 subdomain, and two elements of the Interface domain.

near the active site Cys43. Its 10° tilt relative to the corresponding α-helix in the Npx NADH-binding domain (*39*) can be attributed to an additional salt bridge (Arg56: Asp137) in CoADR. The conformations of the respective Interface domains are the most closely conserved, with the only significant difference being the concerted displacement of a short α-helix and surface-exposed loop (residues 337−349) of CoADR toward the core of the Interface domain, away from the NADPH-binding domain. As with the group 3 PNDOR enzymes Npx and Nox, CoADR is rather less similar to group 1 and 2 PNDORs (*11*, *12*); a representative comparison with the human GR structure results in an rmsd value of 3.4 Å (17% sequence identity).

FAD and NADPH Recognition. Dym and Eisenberg (*10*) summarized four conserved sequence motifs shared by all NAD(P)H-dependent members of the GR_1 subfamily. The CLUSTAL (*40*) alignment for CoADR and other known functional group 3 PNDORs (*41*−*46*) shows that these motifs correspond to CoADR segments Gly8−Glu33 (FAD-1; Figure 4), Gly155−Glu162 (NADPH), Asp231−Pro241 (NADPH-to-FAD-2 interface), and Thr267−Asp277 (FAD-2); with one striking exception, these match the expected sequence fingerprints very closely (*47*, *48*). The FAD coenzymes in CoADR and Npx are bound in nearly identical extended conformations (Figure 3). In both cases the ribityl moiety of FAD is involved in extensive hydrogen-bonding interactions with both side chain and main chain elements of the polypeptide; the redox-active FAD isoalloxazine is buried within the protein core. In Npx Ser9 takes the place of the highly conserved "second" Gly in the dinucleotide-binding motif [DBM (*47*)]; this results in a 1 Å shift of the adenylate phosphate (FAD-PA), as was demonstrated in an earlier comparison of the Npx and GR structures (*33*). Unique to CoADR, a Val residue (Val10) occupies this position (Figure 4), but the even more dramatic shift anticipated for FAD-PA is not observed. Instead, the Val10 side chain is stabilized in a conformation pointing away from the position of FAD-PA to interact with the side chain of Phe40, which in turn adopts a rotamer distinct from that observed for the equivalent Npx Phe39. The other group 3 PNDORs prefer Ser, Asn, or Thr, but not Gly, in the position occupied by CoADR Val10.

NADPH binding to CoADR is expected to be similar to that seen for other NAD(P)H-dependent PNDOR enzymes; CoADR conserves Tyr158, equivalent to the Tyr that sits in the nicotinamide binding pocket in other PNDORs and undergoes a conformational change on NAD(P)H binding (*39*). CoADR also has a Ser160 for Gly substitution within the DBM motif of the NADPH-binding domain, as is the case with several other NADPH-dependent GR_1 subfamily members (*49*).

CoASH Recognition. The CoAS- binding cleft is composed of residues from both subunits of the dimer, as demonstrated by the LIGPLOT (*50*) analysis given in Figure 5A; a shallow channel leads from the protein surface down into the active site, where the Cys43-SSCoA redox center is oriented on the *si* face of the FAD isoalloxazine. The entire CoAS- molecule of chain A has well-defined electron density (Figure 1); CoAS- is bound in an extended conformation, lying close to two α-helices [α1 (residues 12−24) and α11 (residues 294−311)] from the FAD-binding domain, with several additional interactions involving the Interface domain from chain B (Figure 5). There are 12 direct polar interactions involving the extended CoAS- and 9 protein side chains. The adenine base is partially solvent-exposed and participates in hydrophobic interactions with Met432′ on one face, a cation−π (*51*, *52*) stacking interaction (3.5 Å) with the guanidinium moiety of Arg22 on the other face, and a hydrogen bond with Gln19. The 3′-phosphate and ribose of CoAS- are entirely solvent exposed [the k_{cat}/K_m value for 3′-dephospho-CoAD has been reported (*6*) to be 12−13% that of the value for CoAD], with no specific recognition by the CoADR polypeptide except for a single hydrogen bond interaction between Arg22 and the ribose 2′-OH. A

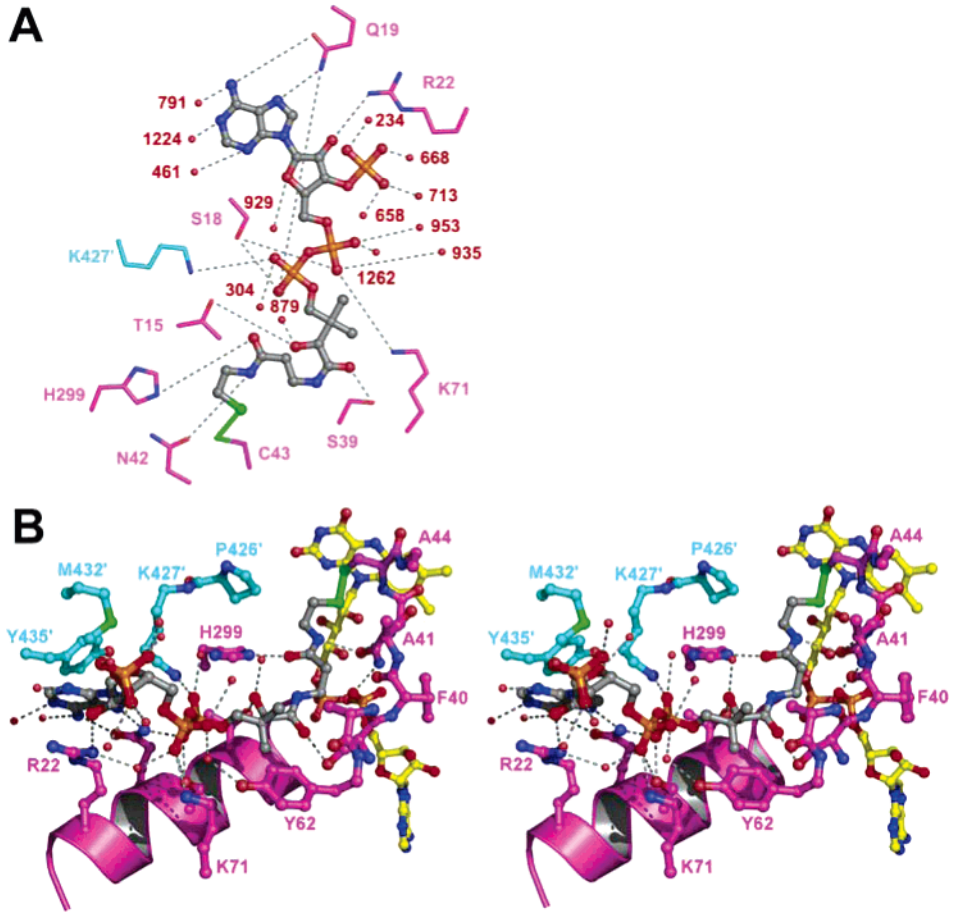

FIGURE 5: Protein−CoAS- interactions in CoADR. (A) LIGPLOT (*50*) representation of protein and WAT interactions with CoAS- in chain A, using default parameters for geometry and hydrogen-bonding distance. Carbon atoms for chain A residues are colored magenta, while those for Lys427′ (chain B) are in cyan. Cys43-SSCoA is color-coded as in Figure 1. WAT are colored red. (B) Stereoview of the Cys43-SSCoA redox center, including protein and direct WAT interactions with CoAS-. FAD and Cys43-SSCoA atoms are color-coded as in Figure 1. Carbon atoms and helix α1 (chain A) are colored magenta; carbon atoms for chain B are colored cyan. WAT are colored red.

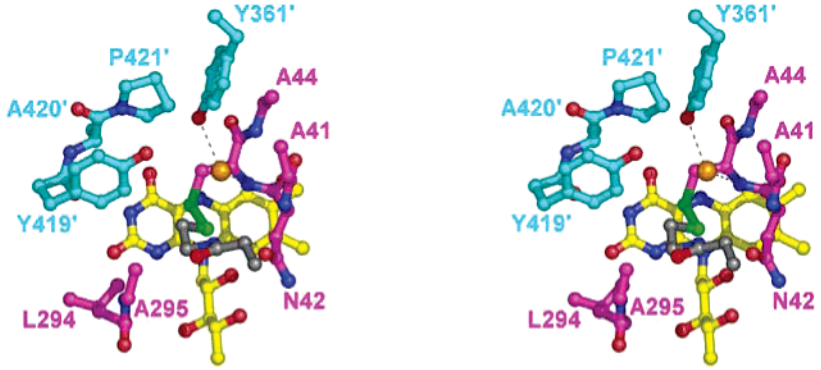

FIGURE 6: Stereoview of the CoADR active site. All residues are color-coded as in Figure 5; the chloride ion is colored orange, and its interactions with Tyr361-O and Cys43-N are indicated by dashes. Portions of the CoAS- and FAD have been omitted for clarity.

bound magnesium ion is located 4.6 Å from the 3′-phosphate, but its presence is clearly related to crystal packing interactions. In contrast, the pantetheine 4′-pyrophosphate is very important for recognition; this moiety is largely buried with all potential hydrogen bonds being satisfied (Figure 5). The negatively charged CoAS- pyrophosphate forms salt bridges with Lys71 and Lys427′ in addition to hydrogen-bonding interactions with the side chains of Ser18 and Gln19 (directly), and with Tyr62-OH, via WAT1262. The nonpolar portion of the pantothenic acid moiety is stabilized by favorable hydrophobic interactions with Phe67, Tyr62, and Ala61, and the more polar element is stabilized by hydrogen bonds with the side chains of His299 and Asn42. A well-ordered chloride ion is positioned adjacent to the Cys43-SSCoA disulfide (Figure 6), 3.8 Å from the CoAS- sulfur, and receives hydrogen bonds from Cys43-N (3.5 Å), Tyr361′-OH (3.1 Å), and WAT1070 (3.2 Å). The presence and position of this monovalent anion in the CoADR active site are fortuitous, in that these favorable interactions could also stabilize the transition state during reduction of the CoAD substrate (see below).

In chain B, the CoAS- moiety is less well ordered but adopts a very similar overall conformation. The electron density for the disulfide and pantetheine elements is well-

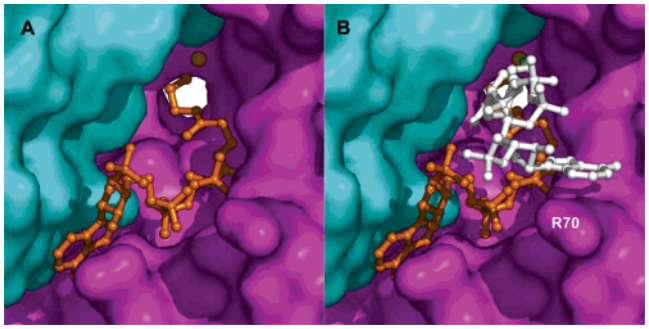

FIGURE 7: Ball-and-stick representations for the CoAS- binding cleft (CoAS-I) and for a modeled CoAS-II. (A) CoADR representation for covalently bound CoAS-I (orange); the chloride ion is also colored orange and occupies the position of the modeled CoAS-II sulfur. (B) The CoAS-II model (white; developed as described in the text) has been added. The C−S bond of the CoAS-II β-mercaptoethylamine moiety is depicted in green. Chains A and B are rendered in magenta and cyan, respectively.

defined, but during refinement strong ($>6\sigma$) difference density indicated the presence of an alternate conformation for the CoAS- pyrophosphate, that has been included in the model. An additional indication of disorder was weak/broken electron density for the CoAS- ribose. This less ordered CoAS- is not involved in crystal packing, so it may more accurately reflect the level of disorder present in CoAS- recognition and binding in solution. However, it is also possible that the difference in the level of CoAS- order is not due to crystal packing but is a subtle reflection of a preexisting asymmetry in the oxidized dimer.

Engel and Wierenga (*53*) have described seven diverse protein folds that productively bind CoASH (as either CoASH or acyl-CoA forms) in both bent and extended conformations. The similarities inferred by comparison of these diverse CoASH-binding proteins include (1) a solvent-exposed 3′-phosphate, with the adenine base pointing toward the protein interior, (2) a hydrogen-bonding interaction between the 6-NH_2 group of the adenine base and the protein, and (3) the presence of at least one salt bridge involving the pyrophosphate. CoADR fulfills all three properties in binding CoAS-, although only CoADR anchors the CoAS- ligand through a disulfide linkage to the protein.

CoASSCoA Recognition. A surface representation of the CoAS- binding site in the dimeric CoADR structure reveals that there is an unoccupied cleft adjacent to each covalently bound CoAS- (here designated CoAS-I, Figure 7). Since the CoADR substrate is the CoASSCoA homodisulfide (CoAD), this cleft might provide for docking of the second CoAS- moiety (CoAS-II) of CoAD during catalysis. Indeed, at the base of the pocket is the chloride ion proposed to represent the position of the CoAS-II sulfur in the enzyme−CoAD complex. Positioning this sulfur atom at the chloride ion site has led to a modeled CoAS-II that has no steric collisions with either protein or bound CoAS- (CoAS-I) atoms. The docked CoAS-II fits well inside the cleft; Arg70 stacks with the adenine base of CoAS-II (mimicking the Arg22−CoAS-I interaction), and the side chain of Asn360′ (*B*-factor = 52 Å^2) can be adjusted to interact with the pyrophosphate moiety of CoAS-II. While this model provides a plausible binding mode for CoAS-II, it awaits experimental confirmation.

Active Site Comparisons with CoADR and Npx. Although Npx Cys42-S_γ aligns near CoADR Cys43-S_γ (C_α displacement of 0.4 Å), the active site residues surrounding Npx Cys42 are not conserved in CoADR (Figure 8), consistent with the significantly different Cys-SOH chemistry involved in Npx versus CoADR catalysis. Npx His10, which is absolutely conserved within the Npx/Nox group (Figure 4), interacts with the Cys42-SOH redox center; H10Q and H10A mutants (*54*) reveal dramatic perturbations in Cys42-SOH → FAD charge-transfer properties, diminished rates of H_2O_2 reactivity with the respective EH_2 form, and increased sensitivity to H_2O_2 inactivation (Cys42-SOH → Cys42-SO_2H/-SO_3H). The Cys42-SOH chemistry facilitated by Npx His10 is not a factor in CoADR catalysis; furthermore, the presence of the extended CoAS- in the CoADR active site dictates the requirement for a small side chain, and Ala11 replaces the His. Similar steric requirements drive the replacements of Npx Tyr13 (Thr in all Noxs) and Tyr60 (absolutely conserved within the Npx/Nox group) with Ala14 and Ala61, respectively, within the CoAS-binding pocket. Leu40, which is absolutely conserved within the Npx/Nox group, is replaced by the small Ala41 side chain in CoADR. Npx Arg303 maintains and orients the neutral His10 side chain (*55*); in CoADR His299 replaces this Arg, satisfying local steric requirements with a smaller side chain volume and also aiding in CoAS- recognition, through a 2.6 Å hydrogen bond from His299-$N_{\epsilon 2}$ to one carbonyl oxygen of the pantetheine moiety. There are two Phe residues (Phe366′ and Phe424′) contributed by the complementary subunit in Npx, which are observed within the catalytic center. Phe424′ also helps to shield the FAD isoalloxazine from solvent and is hydrogen-bonded (Phe424′-O) to FAD-N3F (*33*). These Phe residues are conserved in all known functional Noxs as well, but in CoADR they are replaced with Tyr361′ and Tyr419′; Tyr361′-OH interacts with the active site chloride ion.

In stark contrast to GR (PNDOR group 1), the group 3 CoADR is the only member of the GR_1 subfamily known to catalyze the reduction of a disulfide substrate with a single active site Cys. In GR, His467′ serves a catalytically essential role in protonating the nascent GS-I thiolate as the Cys58-Cys63 protein disulfide forms again (*35*, *56*). In a similar manner, we expect that the CoADR active site provides an acid−base catalyst primed for protonation of the nascent CoAS-II thiolate as the Cys43-SSCoA disulfide is formed. CoADR provides no His equivalent to GR His467′, but a CoADR/GR superposition reveals that the side chain of CoADR Tyr419′ has an orientation similar to that of His467′. Although Tyr419′-OH is 4.2 Å from Cys43-S_γ in the CoADR nonflavin redox center, Tyr361′-OH is only 3.1 Å from the bound chloride ion and is in an orientation optimal for proton donation to a CoAS-II thiolate, modeled into this position. Although individual Y361F and Y419F CoADR mutants have significant activity (8% and 21%, respectively, relative to wild-type CoADR), the Y361F/Y419F double mutant has no measurable activity.[2] Scheme 1 presents a working mechanistic proposal for the combined role(s) of Tyr361′ (and Tyr419′) in CoADR catalysis; this proposal is based primarily on the strong interaction between Tyr361′-OH and the bound chloride ion, taken to mimic the position of the CoAS-II thiol(ate) during CoAD reduction. The SACoADR Tyr mutagenesis data also support this scheme, in a general

[2] J. R. Wallen and A. Claiborne, unpublished experiments.

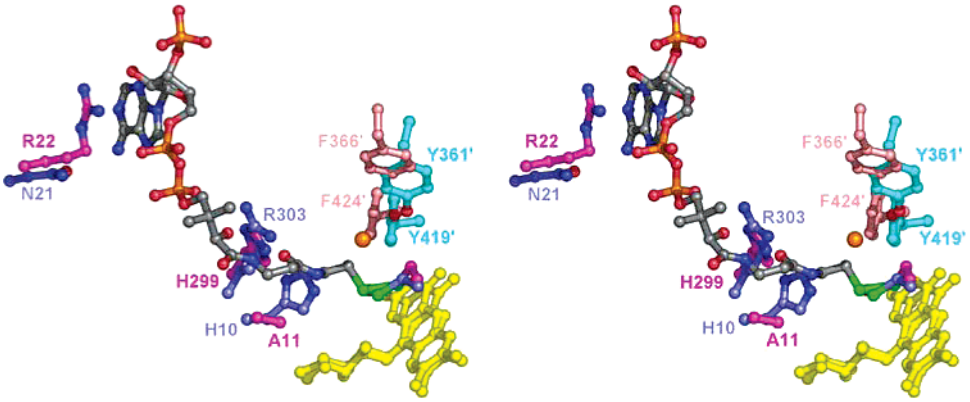

FIGURE 8: Active site overlay, in stereo, for CoADR and Npx. The superposition was performed as described in Figure 3. The two FAD (portions removed for clarity) are given in yellow. CoADR and Npx side chain carbon atoms (each chain A) are rendered in magenta and light blue, respectively. Chain B carbon atoms for CoADR and Npx are colored cyan and beige, respectively. The CoADR active site chloride ion (orange) is included, and CoAS- is color-coded as in Figure 1.

Scheme 1: Proposed Interactions Involving Tyr361′ and Tyr419′ during CoAD Reduction

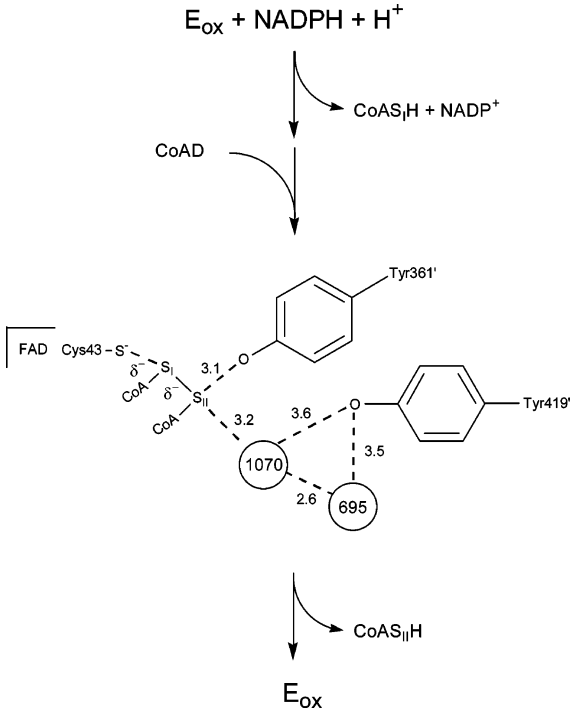

sense. While further detailed kinetic studies have not been performed, structural analyses with the NADH-reduced CoADR (2.25 Å resolution, in refinement) from *Bacillus anthracis* (BACoADR; see below) indicate an altered conformation for Cys42-SH.[2] In the reduced BACoADR−NADH complex, Cys42-S_γ is positioned for good hydrogen bond interactions with both Tyr367′-OH and Tyr425′-OH (equivalent to SACoADR Tyr361′ and Tyr419′, respectively). While more work will be required to elucidate the specific mechanistic roles of the two active site Tyr residues in SACoADR, we would propose from the above that both are involved in formation and stabilization of the Cys43-thiolate and that Tyr361′ also serves the primary role in protonation of the CoAS-II thiolate during CoAD reduction.

Four residues within the Npx Interface domain (Phe424′, Pro426′, Pro431′, and Trp432′) are especially well-suited for roles in shielding the redox-active pyrimidine moiety of FAD from solvent (*33*). All enzymes of the Npx/Nox group conserve the first three residues, although Tyr, Phe, and even Leu are found in place of Trp432′ in the Noxs. The two notable substitutions found in CoADR, within this segment, are Phe → Tyr419′ and Trp → Lys427′; the former substitution is conservative and has already been described. Lys427′ forms a salt bridge (2.7 Å) with the pantetheine pyrophosphate and represents one component of CoAS-recognition. Lys427-N_ϵ is 3.0 Å from His299-$N_{\delta 1}$ and also interacts with WAT47. The interaction involving Lys427′ is complemented by an intersubunit salt bridge between Asp393′ and Lys394, which tightens the junction between helices α13 (residues 391−405) and α13′ within the dimer interface, proximal to the active site. A second intrasubunit salt bridge in this vicinity (Arg393′:Asp428′) also positions helix α13′ with respect to the proximal α15′ helix (residues 428′−436′). These CoADR Interface segments provide the basis for the D-K-R (Asp393−Arg395) and K-D (Lys427−Asp428) sequence motifs (see below) and further serve to differentiate CoADR from the Npx/Nox group.

CoADR Homologues in Bacteria and Archaea. Fahey has classified CoASH as a "common" thiol (*57*), as it occurs in all prokaryotes as well as eukaryotes. GSH, on the other hand, is not produced by the archaea; it is also absent in many bacteria. Harris et al. (*58*) recently reported that CoASH is the major low molecular weight thiol in the hyperthermophilic archaeon *Pyrococcus furiosus*, and the recombinant form of a CoADR from *Pyrococcus horikoshii* has been characterized. The enzyme exhibits a preference for NADPH in the reduction of CoAD, but questions remain regarding both the identity of the nonflavin redox center and the high NAD(P)H oxidase activity observed in the presence of FAD. Boylan et al. (*59*) have more recently demonstrated that the human pathogen *Borrelia burgdorferi* also contains CoASH as the major low molecular weight thiol, and the recombinant *B. burgdorferi* CoADR has been shown to prefer NADH, in contrast to the *S. aureus* enzyme. There is a strong likelihood that CoADR-like enzymes may play similar roles in CoASH-dependent thiol/disulfide redox homeostasis in other prokaryotes as well. The data presented in Figure 4 demonstrate that the *S. aureus* CoADR (SACoADR) sequence can be distinguished from those of the Npx/Nox group. When a *blastp* (*60*) analysis using SACoADR as the query was performed with 288 completed bacterial genomes, the surprising result led to identification of two new classes

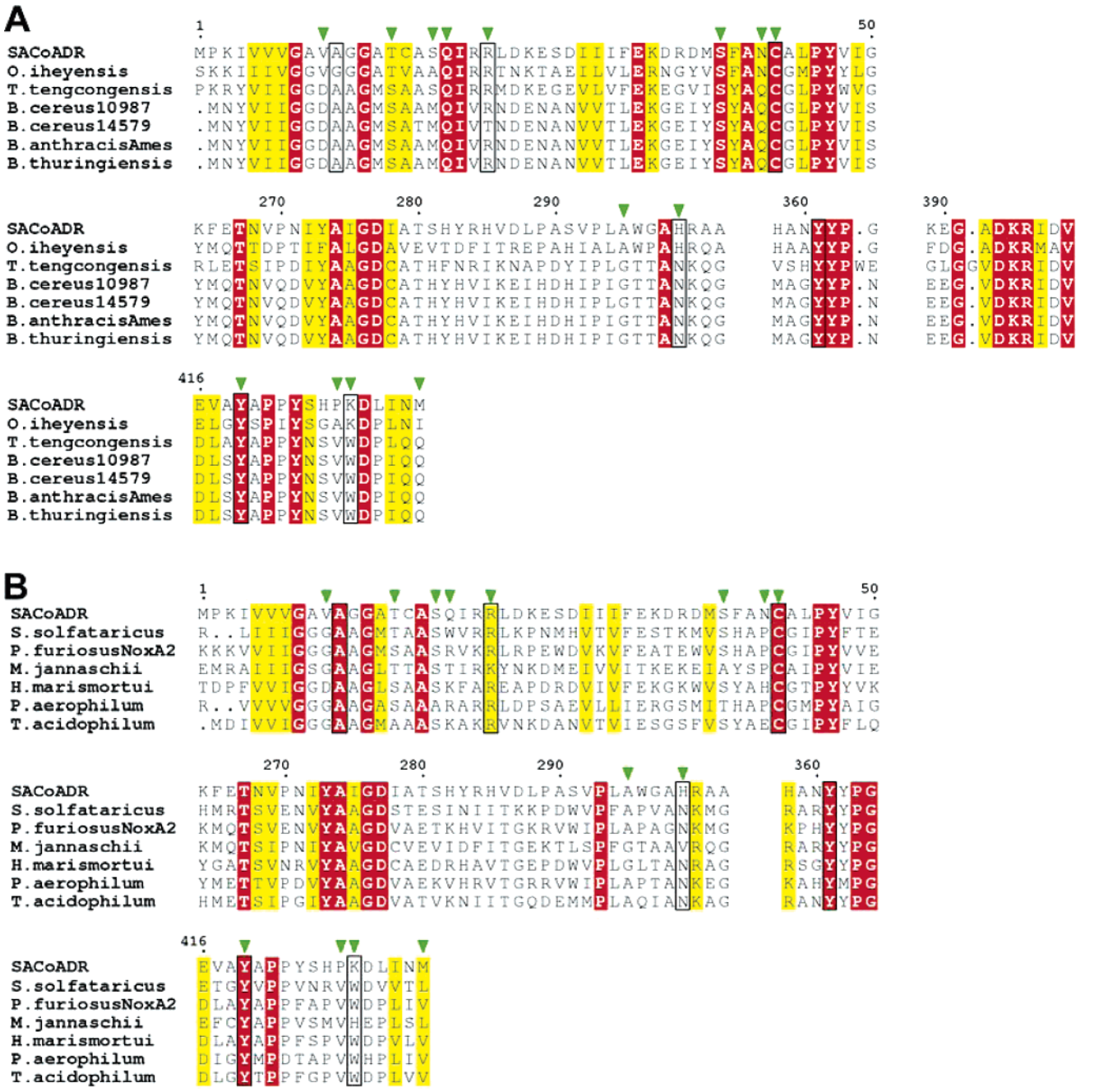

FIGURE 9: Sequence alignments for CoADR and closely related bacterial and archaeal homologues. (A) CoADR homologues with the same domain architecture as SACoADR were identified in the *blastp* analysis described in the text and include proteins from *O. iheyensis* (NP_691780), *T. tengcongensis* (NP_624216), and four species from the *B. cereus* group (NP_977693, NP_831030, NP_843735, and YP_035485). *E* values range from $6e^{-60}$ to $4e^{-67}$. The *E* value for the functional CoADR from *B. burgdorferi* (*59*) is $6e^{-55}$. Segments shown correspond to FAD-1, FAD-2, and three segments from the Interface domain. Other details are as given in Figure 4. (B) A *blastp* analysis of the 26 completed archaeal genomes was performed; *E* values range from $2e^{-45}$ to $4e^{-50}$, and FAD-1, FAD-2, and two Interface segments are shown for proteins from *Sulfolobus solfataricus* (NP_343655), *P. furiosus* [NoxA-2 (*58*, *68*); NP_578915], *Methanocaldococcus jannaschii* (NP_247633), *Haloarcula marismortui* (YP_134552), *Pyrobaculum aerophilum* (NP_559963), and *Thermoplasma acidophilum* (NP_394297). The *E* value for the *P. horikoshii* CoADR (*58*) is $1e^{-41}$. Other details are as given in Figure 4.

of CoADR homologues. Six of the top 25 similarity scores (excluding nine CoADR representatives from *Staphylococcus*) correspond to much longer polypeptides (810−938 residues) sharing a CoADR-rhodanese homology domain [RHD (*61*, *62*)]-SirA-COG2210 multidomain architecture, and 18 of these top scores correspond to CoADR-RHD proteins of ~560 residues. In *E. coli*, the SirA protein TusA/YhhP (*63*, *64*) is a sulfur mediator that interacts with, and accepts sulfane sulfur from, the IscS cysteine desulfurase; this process is essential for 2-thiouridine formation. RHD, SirA, and COG2210 (unknown function) domains each contain one conserved Cys residue; in both rhodanese and TusA, this Cys forms a persulfide intermediate. Notably, the CoADR-RHD proteins are found in category A biodefense pathogens such as *B. anthracis* and *Yersinia pestis*. The crystal structure of the CoADR-RHD protein from *B. anthracis* Ames has been determined in this laboratory,[3]

[3] W. Boles, T. C. Mallett, D. Parsonage, A. Friedlander, and A. Claiborne, unpublished experiments.

confirming that CoAS- is present in the active site, covalently attached to Cys44. The sequences of the CoADR modules from these CoADR-RHD and CoADR-RHD-SirA-COG2210 proteins are 30−39% identical to that of SACoADR.

The third bacterial group of CoADR homologues shares the simple domain organization of SACoADR; there are seven such homologues among the top 32 scores, with sequence identities of 31−35% relative to SACoADR (Figure 9A). *Oceanobacillus iheyensis* is a Gram-positive, *Bacillus*-related spore-forming species noted for its adaptation to highly alkaline and saline environments (*65*); still, it is a strict aerobe. *Thermoanaerobacter tengcongensis* is a Gram-negative, anaerobic hyperthermophile (*66*). *Bacillus cereus* and *Bacillus thuringiensis* are closely related species of the *B. cereus* group, as is *B. anthracis* Ames. The alignment in Figure 9A demonstrates absolute conservation of SACoADR Cys43, Ala41, Tyr361, Tyr419, and Asp428. The D-K-R fingerprint described previously (Asp393−Arg395) is absolutely conserved. Ala11 and Arg22 are very strongly conserved, as is Ala61. Val10, noted earlier as a drastic substitution for the central Gly within the DBM for FAD binding, is replaced by Asp in most cases; this substitution parallels the appearance of Tyr in place of Phe40 as well as the concerted replacements His299 → Asn and Lys427 → Trp. Among the group of SACoADR residues mentioned above, Arg22, His299, and Lys427 were identified in Figure 5 as participating in favorable polar interactions with CoAS-I. Val10 and Tyr419′ are both involved in hydrophobic contacts with the pantetheine moiety. The gene encoding the *B. anthracis* CoADR (BACoADR) is expressed late in sporulation, and the BACoADR protein has been identified in the mature spore (*67*). As a genus, *Bacillus* appears to lack GSH; CoASH is the major low molecular weight thiol in *B. cereus* (*4*) and *B. anthracis*,[4] for example.

In earlier studies (*3*), Setlow and co-workers identified CoASH as the major thiol in *B. megaterium*, and an NADH-dependent CoADR was purified from spores; the apparent k_{cat}/K_m for CoAD was, however, 9-fold lower than that for pantethine 4′,4″-diphosphate. Analysis of the *B. megaterium* draft genome sequence has revealed a single CoADR homologue (33% identity with SACoADR, same domain organization);[5] however, identification with the pantethine diphosphate reductase reported by Swerdlow and Setlow (*3*) awaits further experimental work. For comparison, the functional CoADR from *B. burgdorferi* is 32% identical to SACoADR.

A *blastp* analysis using SACoADR as the query against 26 completed archaeal genomes identified additional putative CoADR enzymes (Figure 9B). Sequence identities with SACoADR range from 27% to 30%, and there is absolute conservation of Ala11, Cys43, Tyr361, and Tyr419. Arg22 and Ala41 are also strongly conserved, but Val10 is now replaced by the consensus Gly in most cases. Although functional information on these archaeal proteins is sparse, the *P. horikoshii* CoADR reported by Harris et al. (*58*) is 92% identical to the *P. furiosus* NoxA-2 included in Figure 9B, and the recombinant NoxA-2 has been reported to exhibit strong CoADR activity in partially purified extracts (*59*). Schut et al. (*68*) also showed that this *noxA-2* gene is highly expressed when elemental sulfur ($S^\circ \rightarrow H_2S$) is present in the growth medium, and Hummel et al. (*5*) have recently reported a dramatic increase in [CoAD]/[CoASH] under these growth conditions. We propose that these enzymes are CoADRs rather than Noxs (as annotated), that CoADR is thus significantly represented in bacteria and archaea, and that the CoASH/CoAD redox system plays an important role in thiol/disulfide homeostasis in these prokaryotes.

[4] C. Paige, J. R. Wallen, G. L. Newton, R. C. Fahey, and A. Claiborne, unpublished experiments.

[5] J. Ravel, personal communication.

ACKNOWLEDGMENT

We thank Dr. James Luba for work in SeMet CoADR preparation and initial crystallization trials and Mr. William Boles for support during data collection at National Synchrotron Light Source and in figure preparation. We also thank Dr. Sunil Ojha for critical reading of the manuscript.

REFERENCES

1. Ortenberg, R., and Beckwith, J. (2003) Functions of thiol-disulfide oxidoreductases in *E. coli*: redox myths, realities, and practicalities, *Antioxid. Redox Signaling 5*, 403−411.
2. Fahey, R. C., and Newton, G. L. (1983) Occurrence of low molecular weight thiols in biological systems, in *Functions of Glutathione: Biochemical, Physiological, Toxicological, and Clinical Aspects* (Larsson, A., et al., Eds.) pp 251−260, Raven Press, New York.
3. Swerdlow, R. D., and Setlow, P. (1983) Purification and characterization of a *Bacillus megaterium* disulfide reductase specific for disulfides containing pantethine 4′,4″-diphosphate, *J. Bacteriol. 153*, 475−484.
4. Newton, G. L., and Fahey, R. C. (1990) Glutathione in prokaryotes, in *Glutathione: Metabolism and Physiological Functions* (Vina, J., Ed.) pp 69−77, CRC Press, Boca Raton, FL.
5. Hummel, C. S., Lancaster, K. M., and Crane, E. J., III (2005) Determination of coenzyme A levels in *Pyrococcus furiosus* and other Archaea: implications for a general role for coenzyme A in thermophiles, *FEMS Microbiol. Lett. 252*, 229−234.
6. delCardayre, S. B., Stock, K. P., Newton, G. L., Fahey, R. C., and Davies, J. E. (1998) Coenzyme A disulfide reductase, the primary low molecular weight disulfide reductase from *Staphylococcus aureus*. Purification and characterization of the native enzyme, *J. Biol. Chem. 273*, 5744−5751.
7. delCardayre, S. B., and Davies, J. E. (1998) *Staphylococcus aureus* coenzyme A disulfide reductase, a new subfamily of pyridine nucleotide-disulfide oxidoreductase. Sequence, expression, and analysis of *cdr*, *J. Biol. Chem. 273*, 5752−5757.
8. Coulter, S. N., Schwan, W. R., Ng, E. Y., Langhorne, M. H., Ritchie, H. D., Westbrock-Wadman, S., Hufnagle, W. O., Folger, K. R., Bayer, A. S., and Stover, C. K. (1998) *Staphylococcus aureus* genetic loci impacting growth and survival in multiple infection environments, *Mol. Microbiol. 30*, 393−404.
9. Schneider, W. P., Ho, S. K., Christine, J., Yao, M., Marra, A., and Hromockyj, A. E. (2002) Virulence gene identification by differential fluorescence induction analysis of *Staphylococcus aureus* gene expression during infection-simulating culture, *Infect. Immun. 70*, 1326−1333.
10. Dym, O., and Eisenberg, D. (2001) Sequence-structure analysis of FAD-containing proteins, *Protein Sci. 10*, 1712−1728.
11. Williams, C. H., Jr. (1992) Lipoamide dehydrogenase, glutathione reductase, thioredoxin reductase, and mercuric ion reductase—a family of flavoenzyme transhydrogenases, in *Chemistry and Biochemistry of Flavoenzymes* (Muller, F., Ed.) pp 121−211, CRC Press, Boca Raton, FL.
12. Argyrou, A., and Blanchard, J. S. (2004) Flavoprotein disulfide reductases: advances in chemistry and function, *Prog. Nucleic Acid Res. Mol. Biol. 78*, 89−142.
13. Claiborne, A., Mallett, T. C., Yeh, J. I., Luba, J., and Parsonage, D. (2001) Structural, redox, and mechanistic parameters for cysteine-sulfenic acid function in catalysis and regulation, *Adv. Protein Chem. 58*, 215−276.

14. Luba, J., Charrier, V., and Claiborne, A. (1999) Coenzyme A-disulfide reductase from *Staphylococcus aureus*: evidence for asymmetric behavior on interaction with pyridine nucleotides, *Biochemistry 38*, 2725−2737.
15. Jancarik, J., and Kim, S. H. (1991) Sparse-matrix sampling—a screening method for crystallization of proteins, *J. Appl. Crystallogr. 24*, 409−411.
16. Wood, Z. A., Poole, L. B., and Karplus, P. A. (2001) Structure of intact AhpF reveals a mirrored thioredoxin-like active site and implies large domain rotations during catalysis, *Biochemistry 40*, 3900−3911.
17. Leslie, A. G. W. (1992) Recent changes to the MOSFLM package for processing film and image plate data, Joint CCP4 + ESF-EAMCB Newsletter on Protein Crystallography.
18. Kabsch, W. (1988) Automatic-indexing of rotation diffraction patterns, *J. Appl. Crystallogr. 21*, 67−71.
19. Diederichs, K., and Karplus, P. A. (1997) Improved R-factors for diffraction data analysis in macromolecular crystallography, *Nat. Struct. Biol. 4*, 269−275.
20. (1994) The CCP4 suite: programs for protein crystallography, *Acta Crystallogr. D50*, 760−763.
21. Terwilliger, T. C., and Berendzen, J. (1999) Automated MAD and MIR structure solution, *Acta Crystallogr. D55*, 849−861.
22. de La Fortelleqq, E., and Bricogne, G. (1997) Maximum-likelihood heavy-atom parameter refinement for multiple isomorphous replacement and multiwavelength anomalous diffraction methods, *Methods Enzymol. 276*, 472−494.
23. Cowtan, K., and Main, P. (1998) Miscellaneous algorithms for density modification, *Acta Crystallogr. D54*, 487−493.
24. Levitt, D. G. (2001) A new software routine that automates the fitting of protein X-ray crystallographic electron-density maps, *Acta Crystallogr. D57*, 1013−1019.
25. Jones, T. A., Zou, J. Y., Cowan, S. W., and Kjeldgaard, M. (1991) Improved methods for building protein models in electron-density maps and the location of errors in these models, *Acta Crystallogr. A47*, 110−119.
26. Pflugrath, J. W. (1999) The finer things in X-ray diffraction data collection, *Acta Crystallogr. D55*, 1718−1725.
27. Brunger, A. T., Adams, P. D., Clore, G. M., DeLano, W. L., Gros, P., Grosse-Kunstleve, R. W., Jiang, J. S., Kuszewski, J., Nilges, M., Pannu, N. S., Read, R. J., Rice, L. M., Simonson, T., and Warren, G. L. (1998) Crystallography and NMR system: A new software suite for macromolecular structure determination, *Acta Crystallogr. D54*, 905−921.
28. Kleywegt, G. J., and Jones, T. A. (1998) Databases in protein crystallography, *Acta Crystallogr. D54*, 1119−1131.
29. Holm, L., and Sander, C. (1993) Protein structure comparison by alignment of distance matrices, *J. Mol. Biol. 233*, 123−138.
30. Kabsch, W. (1976) Solution for best rotation to relate 2 sets of vectors, *Acta Crystallogr. A32*, 922−923.
31. Navaza, J. (1994) AMORE—an automated package for molecular replacement, *Acta Crystallogr. A50*, 157−163.
32. Luzzati, V. (1952) Traitement statistique des erreurs dans la determination des structures cristallines, *Acta Crystallogr. 5*, 802−810.
33. Stehle, T., Ahmed, S. A., Claiborne, A., and Schulz, G. E. (1991) Structure of NADH peroxidase from *Streptococcus faecalis* 10C1 refined at 2.16 Å resolution, *J. Mol. Biol. 221*, 1325−1344.
34. Karplus, P. A., and Schulz, G. E. (1987) Refined structure of glutathione reductase at 1.54 Å resolution, *J. Mol. Biol. 195*, 701−729.
35. Karplus, P. A., and Schulz, G. E. (1989) Substrate binding and catalysis by glutathione reductase as derived from refined enzyme: substrate crystal structures at 2 Å resolution, *J. Mol. Biol. 210*, 163−180.
36. Mittl, P. R. E., and Schulz, G. E. (1994) Structure of glutathione reductase from *Escherichia coli* at 1.86 Å resolution: comparison with the enzyme from human erythrocytes, *Protein Sci. 3*, 799−809.
37. Sandalova, T., Zhong, L., Lindqvist, Y., Holmgren, A., and Schneider, G. (2001) Three-dimensional structure of a mammalian thioredoxin reductase: implications for mechanism and evolution of a selenocysteine-dependent enzyme, *Proc. Natl. Acad. Sci. U.S.A. 98*, 9533−9538.
38. Rossmann, M. G., Moras, D., and Olsen, K. W. (1974) Chemical and biological evolution of nucleotide-binding protein, *Nature 250*, 194−199.
39. Stehle, T., Claiborne, A., and Schulz, G. E. (1993) NADH binding site and catalysis of NADH peroxidase, *Eur. J. Biochem. 211*, 221−226.
40. Chenna, R., Sugawara, H., Koike, T., Lopez, R., Gibson, T. J., Higgins, D. G., and Thompson, J. D. (2003) Multiple sequence alignment with the Clustal series of programs, *Nucleic Acids Res. 31*, 3497−3500.
41. Ross, R. P., and Claiborne, A. (1991) Cloning, sequence and overexpression of NADH peroxidase from *Streptococcus faecalis* 10C1. Structural relationship with the flavoprotein disulfide reductases, *J. Mol. Biol. 221*, 857−871.
42. Ferretti, J. J., McShan, W. M., Ajdic, D., Savic, D. J., Savic, G., Lyon, K., Primeaux, C., Sezate, S., Suvorov, A. N., Kenton, S., Lai, H. S., Lin, S. P., Qian, Y., Jia, H. G., Najar, F. Z., Ren, Q., Zhu, H., Song, L., White, J., Yuan, X., Clifton, S. W., Roe, B. A., and McLaughlin, R. (2001) Complete genome sequence of an M1 strain of *Streptococcus pyogenes*, *Proc. Natl. Acad. Sci. U.S.A. 98*, 4658−4663.
43. Auzat, I., Chapuy-Regaud, S., Le Bras, G., Dos Santos, D., Ogunniyi, A. D., Le Thomas, I., Garel, J.-R., Paton, J. C., and Trombe, M.-C. (1999) The NADH oxidase of *Streptococcus pneumoniae*: its involvement in competence and virulence, *Mol. Microbiol. 34*, 1018−1028.
44. Matsumoto, J., Higuchi, M., Shimada, M., Yamamoto, Y., and Kamio, Y. (1996) Molecular cloning and sequence analysis of the gene encoding the H_2O-forming NADH oxidase gene from *S. mutans*, *Biosci. Biotechnol. Biochem. 60*, 39−43.
45. Ross, R. P., and Claiborne, A. (1992) Molecular cloning and analysis of the gene encoding the NADH oxidase from *Streptococcus faecalis* 10C1. Comparison with NADH peroxidase and the flavoprotein disulfide reductases, *J. Mol. Biol. 227*, 658−671.
46. Stanton, T. B., and Sellwood, R. (1999) Cloning and characteristics of a gene encoding NADH oxidase, a major mechanism for oxygen metabolism by the anaerobic spirochete, *Brachyspira (Serpulina) hyodysenteriae*, *Anaerobe 5*, 539−546.
47. Wierenga, R. K., Terpstra, P., and Hol, W. G. J. (1986) Prediction of the occurrence of the ADP-binding beta-alpha-beta-fold in proteins, using an amino acid sequence fingerprint, *J. Mol. Biol. 187*, 101−107.
48. Eggink, G., Engel, H., Vriend, G., Terpstra, P., and Witholt, B. (1990) Rubredoxin reductase of *Pseudomonas oleovorans*. Structural relationship to other flavoprotein oxidoreductases based on one NAD and two FAD fingerprints, *J. Mol. Biol. 212*, 135−142.
49. Scrutton, N. S., Berry, A., and Perham, R. N. (1990) Redesign of the coenzyme specificity of a dehydrogenase by protein engineering, *Nature 343*, 38−43.
50. Wallace, A. C., Laskowski, R. A., and Thornton, J. M. (1995) LIGPLOT: a program to generate schematic diagrams of protein-ligand interactions, *Protein Eng. 8*, 127−134.
51. Dougherty, D. A. (1996) Cation-pi interactions in chemistry and biology: a new view of benzene, Phe, Tyr, and Trp, *Science 271*, 163−168.
52. Biot, C., Buisine, E., Kwasigroch, J. M., Wintjens, R., and Rooman, M. (2002) Probing the energetic and structural role of amino acid/nucleobase cation-pi interactions in protein-ligand complexes, *J. Biol. Chem. 277*, 40816−40822.
53. Engel, C., and Wierenga, R. (1996) The diverse world of coenzyme A binding proteins, *Curr. Opin. Struct. Biol. 6*, 790−797.
54. Crane, E. J., III, Parsonage, D., and Claiborne, A. (1996) The active-site histidine-10 of enterococcal NADH peroxidase is not essential for catalytic activity, *Biochemistry 35*, 2380−2387.
55. Mande, S. S., Parsonage, D., Claiborne, A., and Hol, W. G. J. (1995) Crystallographic analyses of NADH peroxidase Cys42Ala and Cys42Ser mutants: active site structures, mechanistic implications, and an unusual environment of Arg303, *Biochemistry 34*, 6985−6992.
56. Rietveld, P., Arscott, L. D., Berry, A., Scrutton, N. S., Deonarain, M. P., Perham, R. N., and Williams, C. H., Jr. (1994) Reductive and oxidative half-reactions of glutathione reductase from *Escherichia coli*, *Biochemistry 33*, 13888−13895.
57. Fahey, R. C. (2001) Novel thiols of prokaryotes, *Annu. Rev. Microbiol. 55*, 333−356.
58. Harris, D. R., Ward, D. E., Feasel, J. M., Lancaster, K. M., Murphy, R. D., Mallet, T. C., and Crane, E. J., III (2005) Discovery and characterization of a coenzyme A disulfide reductase from *Pyrococcus horikoshii*. Implications for this disulfide metabolism of anaerobic hyperthermophiles, *FEBS J. 272*, 1189−1200.

59. Boylan, J. A., Hummel, C. S., Benoit, S., Garcia-Lara, J., Treglown-Downey, J., Crane, E. J., III, and Gherardini, F. C. (2006) *Borrelia burgdorferi* bb0728 encodes a coenzyme A disulfide reductase whose function suggests a role in intracellular redox and oxidative stress response, *Mol. Microbiol. 59*, 475−486.
60. Altschul, S. F., Gish, W., Miller, W., Myers, E. W., and Lipman, D. J. (1990) Basic local alignment search tool, *J. Mol. Biol. 215*, 403−410.
61. Palenchar, P. M., Buck, C. J., Cheng, H., Larson, T. J., and Mueller, E. G. (2000) Evidence that ThiI, an enzyme shared between thiamin and 4-thiouridine biosynthesis, may be a sulfurtransferase that proceeds through a persulfide intermediate, *J. Biol. Chem. 275*, 8283−8286.
62. Matthies, A., Rajagopalan, K. V., Mendel, R. R., and Leimkuhler, S. (2004) Evidence for the physiological role of a rhodanese-like protein for the biosynthesis of the molybdenum cofactor in humans, *Proc. Natl. Acad. Sci. U.S.A. 101*, 5946−5951.
63. Ikeuchi, Y., Shigi, N., Kato, J., Nishimura, A., and Suzuki, T. (2006) Mechanistic insights into sulfur relay by multiple sulfur mediators involved in thiouridine biosynthesis at tRNA wobble positions, *Mol. Cell 21*, 97−108.
64. Katoh, E., Hatta, T., Shindo, H., Ishii, Y., Yamada, H., Mizuno, T., and Yamazaki, T. (2000) High precision NMR structure of YhhP, a novel *Escherichia coli* protein implicated in cell division, *J. Mol. Biol. 304*, 219−229.
65. Lu, J., Nogi, Y., and Takami, H. (2001) *Oceanobacillus iheyensis* gen. nov., sp. nov., a deep-sea extremely halotolerant and alkaliphilic species isolated from a depth of 1050 m on the Iheya Ridge, *FEMS Microbiol. Lett. 205*, 291−297.
66. http://btn.genomics.org.cn:8080/tten/. (2004) *Thermoanaerobacter tengcongensis*.
67. Liu, H., Bergman, N. H., Thomason, B., Shallom, S., Hazen, A., Crossno, J., Rasko, D. A., Ravel, J., Read, T. D., Peterson, S. N., Yates, J., III, and Hanna, P. C. (2004) Formation and composition of the *Bacillus anthracis* endospore, *J. Bacteriol. 186*, 164−178.
68. Schut, G. J., Zhou, J., and Adams, M. W. W. (2001) DNA microarray analysis of the hyperthermophilic archaeon *Pyrococus furiosus*: evidence for a new type of sulfur-reducing enzyme complex, *J. Bacteriol. 183*, 7027−7036.

BI061139A